Simulation

Simulation: Transactions of the Society for Modeling and Simulation International
87(5) 385–405

DOI: 10.1177/0037549710379481
sim.sagepub.com

Integrating epidemic dynamics with daily commuting networks: building a multilayer framework to assess influenza A (H1N1) intervention policies

Yu-Shiuan Tsai[1], Chung-Yuan Huang[2], Tzai-Hung Wen[3], Chuen-Tsai Sun[1] and Muh-Yong Yen[4]

Abstract

We describe an innovative simulation framework that combines daily commuting network data with a commonly used population-based transmission model to assess the impacts of various interventions on epidemic dynamics in Taiwan. Called the *Multilayer Epidemic Dynamics Simulator* (MEDSim), our proposed framework has four contact structures: within age group, between age groups, daily commute, and nationwide interaction. To test model flexibility and generalizability, we simulated outbreak locations and intervention scenarios for the 2009 swine-origin influenza A (H1N1) epidemic. Our results indicate that lower transmission rates and earlier intervention activation times did not reduce total numbers of infected cases, but did delay peak times. When the transmission rate was decreased by a minimum of 70%, significant epidemic peak delays were observed when interventions were activated before new case number 50; no significant effects were noted when the transmission rate was decreased by less than 30%. Observed peaks occurred more quickly when initial outbreaks took place in urban rather than rural areas. According to our results, the MEDSim provides insights that reflect the dynamic processes of epidemics under different intervention scenarios, thus clarifying the effects of complex contact structures on disease transmission dynamics.

Keywords

computer simulation, epidemic dynamics, geographic information system, multilayer model, travel network

1. Introduction

After emerging in Mexico in April of 2009, the swine-origin H1N1 influenza virus rapidly spread worldwide. In June of that year, the World Health Organization issued its highest possible pandemic alert: level 6.[1] Influenza researchers and epidemiologists have focused on two spreading factors: age group (determining post-infection symptoms)[2–7] and adult travel (determining routes by which viruses spread). Since individuals in the same age group tend to have similar epidemic characteristics, age group has been proposed as a distinguishing condition in terms of population compartmentalization.[2–6,8] Children and adolescents generally have better resistance to contagious diseases than individuals age 65 and older. However, the Mexican population segment that was most affected by the H1N1 virus consisted of youths below the age of 15; of all individuals affected by the first infection wave, 61% were children and 29% adults.[9] Since novel influenza viruses are known to cause greater morbidity among children,[10] the youngest age group served as the main focus of H1N1 intervention efforts.

[1]Department of Computer Science, National Chiao Tung University, Taiwan.
[2]Department of Computer Science and Information Engineering and Research Center for Emerging Viral Infections, Chang Gung University, Taiwan.
[3]Department of Geography and Infectious Disease Research and Education Center, National Taiwan University, Taiwan.
[4]Infectious Disease Section, Taipei City Hospital, Taiwan.

Corresponding author:
Tzai-Hung Wen, Department of Geography and Infectious Disease Research and Education Center, National Taiwan University, 1 Sec. 4, Roosevelt Road, Taipei 10617, Taiwan
Email: wenthung@ntu.edu.tw

Many researchers have used age structure to capture heterogeneity when modeling epidemic dynamics,[3,5,7] with some integrating compartmental models consisting of different age groups to identify potential impacts of specific populations and temporal epidemic trends.[7] Childhood diseases, such as rotavirus infections, have been used to assess the efficacy potential of various vaccination strategies,[5] and transmission threshold and stability have been the focuses of epidemic simulations involving specific age structures.[3]

Another important factor in modeling epidemic dynamics is population movement. Over the past three decades Taiwan has experienced a rapid increase in the number of commuters for work and other purposes, particularly among young adults[11] – a phenomenon perceived as supporting the spread of viruses over long distances within the country.[8] Commuting is marked by strong spatial-temporal regularity: regardless of travel distance or time, most commuters follow simple and repetitive patterns.[12] These patterns are receiving considerable attention from researchers studying the spreading dynamics of diseases and viruses,[13] the clustering characteristics of epidemic diseases at the beginning of a breakout,[14,15] and the targeting of vaccinations, quarantining, and other public health policies.[16–19]

The two most commonly used approaches to modeling epidemic spreading dynamics are population based and network oriented. In population-based approaches, hosts sharing the same symptoms are modeled or grouped in terms of limited numbers of classes (also known as compartments) that researchers analyze and compare.[2–7] Combinations of classes are used to model and analyze population dynamics. For example, the *Susceptible*, *Latent*, *Infectious*, or *Recovered* (SLIR)[20] model gives individuals one of four infection statuses and differential equations are used to study system dynamics in terms of transitions between epidemiological phases. Depending on whether removed individuals can become susceptible a second time, diseases can be modeled as SLIR or SLIRS cycles.

Network-oriented approaches emphasize individual heterogeneity, interactions among individuals, and network structure.[21,22,40] Individuals in a network are represented as nodes, and interactions between them as links. Network nodes can be used to represent the characteristics of individuals, locations, neighborhoods, or cities, and models can incorporate the temporal dynamics of these features. Time frames for links between two nodes can be preferentially defined[23] – an approach commonly used to represent group structures for individuals exhibiting interaction or relationship patterns.[24–27] Network-oriented approaches are suitable for capturing complex contact patterns among individuals, exploring epidemic dynamics, and assessing the efficacies of public health policies.[19,22,28,29] Lattice networks have been used to determine distance relationships between individuals. In contrast, random networks support features associated with casual contacts among mobile individuals and the low degree of separation commonly observed in social networks.[30–32] Some researchers incorporate more realistic underlying networks (e.g. daily contact networks) when modeling interaction behaviors.[30–32] These approaches are viewed as reliable for investigating epidemics, with the transmission dynamics of specific network models being manipulated to investigate the spread of emerging infectious diseases.[33,39] The topological features of social networks have recently been found to exert considerable influence on the transmission dynamics and critical thresholds of infectious diseases, thus supporting the subtle analyses that network-oriented models are incapable of.[4,13,28,34]

Population-based and network-oriented approaches respectively emphasize large-scale population-level and individual-level perspectives. Each has its own limitations. Population-based approaches are suitable for discussing dynamic variation across individuals in the same compartment, but they are weak in terms of modeling individual heterogeneity and addressing human travel networks.[22,30] Since individuals are modeled as groups, any two group members are assumed to have a direct connection, which is not true in the real world. Furthermore, movement and activity are location dependent; therefore, phenomena cannot be simulated by a population-based approach that assumes a homogeneous population distribution. In contrast, network-oriented approaches may be appropriate for introducing individual heterogeneity, but they are computation intensive and time consuming when simulating the behaviors of individuals with multiple attributes in large-scale social environments.[17,30] Many efforts have been made to match individual and population behaviors with heterogeneity and computation requirements when studying epidemic dynamics.[35–37]

Here we will propose a multilayer simulation framework that combines daily commuting networks and a commonly used population-based transmission model for simulating epidemic dynamics. We used the 2008–2009 seasonal influenza A and 2009 swine-origin influenza A (H1N1) outbreaks to estimate model parameters. We then assessed the potential impacts of different outbreak locations and interventions on the Taiwan-wide epidemic dynamics of swine-origin influenza A, including intervention timing and different combinations of public health responses.

2. Multilayer epidemic dynamic simulation

To analyze the spreading dynamics of epidemic diseases in detail, we established a top-down simulation

framework and implemented a prototype of our Multilayer Epidemic Dynamics Simulator (MEDSim). The MEDSim integrates population-based and network-oriented approaches to capturing complex demographic, geographic, and biological properties, including human movement patterns and disease progression (Figure 1). Based on the observation that epidemic dynamics in large populations are similar to those found in deterministic systems,[16] we established a deterministic framework for our MEDSim model. As shown in Figure 2, layer 1 individuals within the same location are organized according to age group;

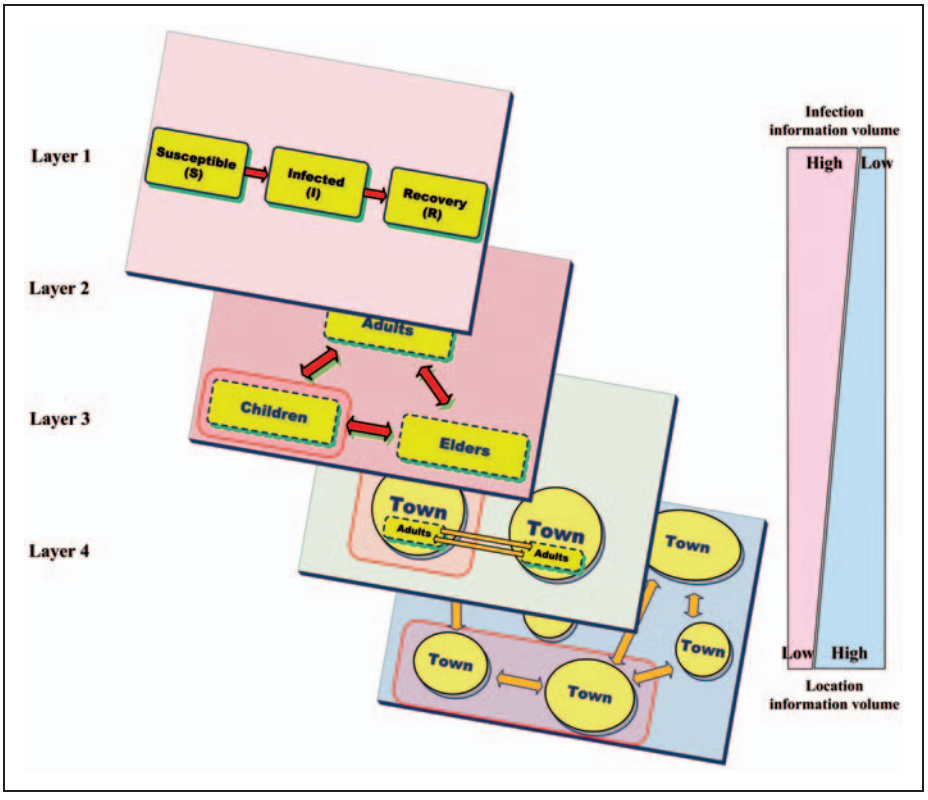

Figure 1. The MEDSim concept. Infection information usage is highest in layer 1 and lowest in layer 4, the opposite of location information.

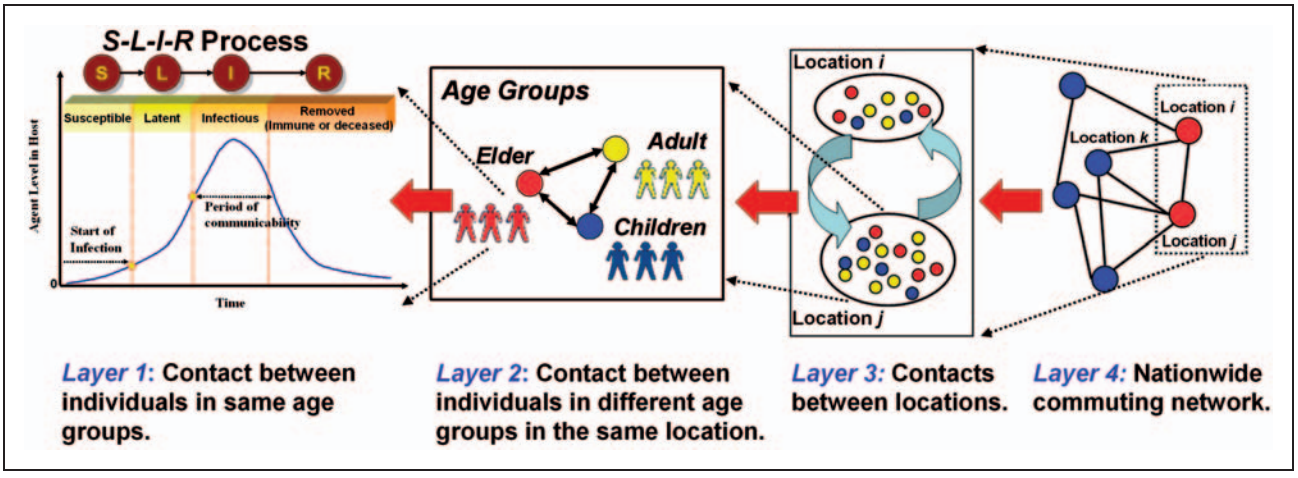

Figure 2. MEDSim framework.

a population-based approach is used to model the transmission dynamics of each group. The layer 2 focus is on contact patterns and interactions between different age groups within the same location. The effects of regional interactions on human travel networks are added to layer 3 by incorporating population density and commuting volume between any two locations. In layer 4, a network-oriented approach is used to incorporate a geographic information system (GIS) for constructing human travel networks on a national scale, with nodes representing locations on commuting routes and links representing movement between them.

Due to its ability to comprehensively integrate multilayer structures to generate dynamic spatial and temporal processes, we used Mathworks MATLAB to implement our MEDSim framework as a numerical computation kernel. By using Microsoft Excel to organize census and transportation data, policy makers, health professionals, and others who have less experience with specialized computer software will be able to generate simulation scenarios with minimal assistance.

2.1. Layer 1: Within age groups

We used the four-state SLIR epidemiological model to represent different infection stages among individuals in the same age group in the same location. Individual epidemic status is initially set at *S*usceptible (vulnerable to infection but not yet infected), followed by *L*atent (infected but unable to infect others), *I*nfectious (capable of infecting other individuals), and *R*emoved (i.e. recovered, deceased, or otherwise not posing any further threat). The numbers of pathogens that Susceptible-to-Latent hosts carry are insufficient for active transmission to other Susceptible hosts, but these numbers eventually reach levels where hosts become Infectious, begin to infect other Susceptible hosts, and eventually move toward a Removed status. The dynamics of the four epidemic states over time are expressed as Equations (1a)–(1d), which have the following features.

1. At time t, the population of interest is divided into four compartments ($S(t)$, $L(t)$, $I(t)$, and $R(t)$) corresponding to the SLIR model's four epidemic states. Since the SLIR model is a closed system, $S(t) + L(t) + I(t) + R(t) = N$, with N a constant representing the entire population.
2. Transmission rate β is a constant representing how fast Susceptible individuals become Infected and acquire a Latent status.
3. Latent rate θ is a constant used to determine transformation speed from Latent to Infected.
4. Removed rate α is a constant used to determine transformation speed from Infected to Recovered.

Ordinary differential equations can be used to express the SLIR model as follows:

$$\frac{dS(t)}{dt} = -\beta S(t)I(t)/N \tag{1a}$$

$$\frac{dL(t)}{dt} = -\theta L(t) + \beta S(t)I(t)/N \tag{1b}$$

$$\frac{dI(t)}{dt} = -\alpha I(t) + \theta L(t) \tag{1c}$$

$$\frac{dR(t)}{dt} = \alpha I(t) \tag{1d}$$

Figures 3(a) and (b) respectively present the concept and a flowchart of our model's first layer. Note our modification in the interest of taking into consideration self-motivated hospitalization (i.e. those individuals who visit hospitals or clinics during an influenza outbreak regardless of their infection status). Depending on diagnostic accuracy, some are confirmed as infectious and receive medical treatment in advance, thus altering transmission and removed rates for certain populations. To integrate this factor into the model, we propose adding three features: (a) an investigation constant s representing the percentage of a population that goes to a hospital or clinic in advance of becoming ill; (b) a detection constant c, used to determine the percentage of a population confirmed as infectious; and (c) a time delay constant T, indicating the amount of time between a patient with symptoms visiting a hospital or clinic and the time his or her infection is confirmed. The default values of parameters s and c are both 0.6 (Table 1), meaning that 60% of the infected population is prone to visiting hospitals and/or clinics for medical advice, and 60% of those visitors are correctly diagnosed as carrying the pathogen. The default value of parameter T is 3 (Table 1), meaning that it takes three days to confirm that a hospital or clinic patient with symptoms is infected with the pathogen. In simulations, correctly diagnosed patients are equivalent to confirmed cases in real-world influenza surveillance systems.

In consideration of preventive health care, we added a feature in which individuals with an L status are moved to either an I_1 (infected and prone to visiting hospitals and/or clinics for medical advice) or I_2 (infected but not prone to visiting hospitals and/or clinics) status, based on whether or not they actually visit a hospital or clinic; this feature is expressed as investigation proportion s. I_1 individuals are identified as either I_{11} (correctly diagnosed as carrying the pathogen) or I_{12} (incorrectly diagnosed as carrying the pathogen – in other words, false negatives); this is expressed as detection proportion c. Note that regardless of

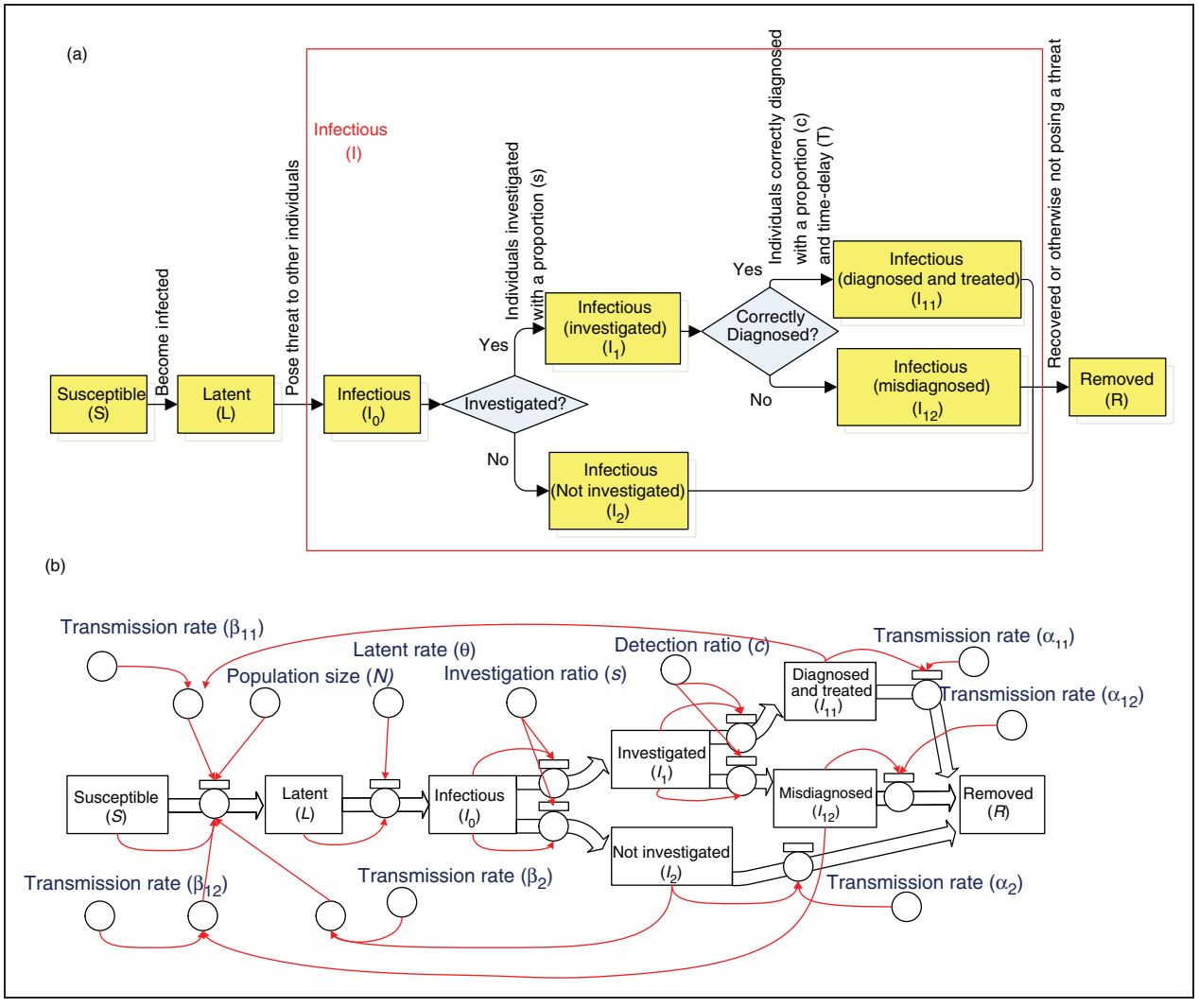

Figure 3. (a) Modified SLIR model layer 1 concept. (b) Modified SLIR model layer 1 flowchart.

positive or negative diagnoses, a T period of time must elapse prior to confirmation. The difference between state I_{11} and either I_2 or I_{12} is the transmission rate. I_{11}, I_{12}, and I_2 all eventually change to state R.

The extended SLIR model can be expressed as

$$\frac{dS(t)}{dt} = -S(t)(\beta_2 I_2(t) + \beta_{11} I_{11}(t) + \beta_{12} I_{12}(t))/N \quad (2a)$$

$$\frac{dL(t)}{dt} = -\theta L(t) + S(t)(\beta_2 I_2(t) + \beta_{11} I_{11}(t) + \beta_{12} I_{12}(t))/N \quad (2b)$$

$$\frac{dI_0(t)}{dt} = -I_0(t) + \theta L(t) \quad (2c)$$

$$\frac{dI_1(t)}{dt} = -I_1(t-T) + sI_0(t) \quad (2d)$$

$$\frac{dI_2(t)}{dt} = -\alpha_2 I_2(t) + (1-s)I_0(t) \quad (2e)$$

$$\frac{dI_{11}(t)}{dt} = -\alpha_{11} I_{11}(t) + cI_1(t-T) \quad (2f)$$

$$\frac{dI_{12}(t)}{dt} = -\alpha_{12} I_{12}(t) + (1-c)I_1(t-T) \quad (2g)$$

$$\frac{dR(t)}{dt} = \alpha_{11} I_{11}(t) + \alpha_{12} I_{12}(t) + \alpha_2 I_2(t) \quad (2h)$$

2.2. Layer 2: Among age groups

Depending on age range, individual infection properties differ in terms of epidemic parameters such as transmission and removed rates. We considered two age-related

Table 1. MEDSim parameters

Category	Layer	Attribute	Symbol	Description
Epidemic	1	*Transmission rate*	β^i_{11pp}	Transmission rate from investigated/diagnosed/treated age group p to same age group in town i
			β^i_{12pp}	Transmission rate from investigated/misdiagnosed age group p to same age group in town i
			β^i_{2pp}	Transmission rate from non-investigated age group p to same age group in town i
		Latent rate	θ^i_p	Latent rate of age group p in town i
		Removed rate	α^i_{11p}	Removed rate of investigated/diagnosed/treated age group p in town i
			α^i_{12p}	Removed rate of misdiagnosed age group p in town i
			α^i_{2p}	Removed rate of non-investigated age group p in town i
		Investigation ratio	s^i_p	Investigated proportion of age group p in town i (Default: 0.6)
		Detection ratio	c^i_p	Correctly diagnosed proportion of age group p in town i (Default: 0.6)
		Delay time	T	Time between investigation and correct diagnosis (Default: 3)
	2	*Transmission rate*	β^i_{11xy}	Transmission rate from investigated/diagnosed/treated age group p and same age group q in town i
			β^i_{12xy}	Transmission rate from misdiagnosed age-group p and same age group q in town i
			β^i_{2xy}	Transmission rate from the non-investigated age group p and same age group q in town i
Location	2	*Relative percentage*	χ^i_p	Age group p as a percentage of town i population. (*Source*: ROC Interior Ministry)
	3	*Determination*	$\sigma(p)$	Binary value for commuter age level (Default: adult)
		Relative density	d^i	Population of town i as a percentage of the largest town's population (*Source*: ROC Interior Ministry)
		Commuting weight	$w_{j,i}$	Number of commuters from town i to town j (*Source*: ROC Institute of Transportation)
	4	*Intercity rate*	η^i	Average number of daily contacts among individuals in location i (Default: 0.8)

features: the transmission rates β_{11pq}, β_{12pq}, and β_{2pq}, which represent cross-age group infections, and the relative percentage χ_p of age level, which affects the potential for cross-age infections. To distinguish among parameters for individuals in different age groups, we also added a subscript to each Equation (2) parameter (with the exception of T) – for example, we changed parameter $S(t)$ to $S_p(t)$ for age level p. We assumed three age levels when analyzing H1N1: children (from birth to 14), adults (15–64), and seniors (65 and older). Transmission rates between age levels were differentiated to capture the complexity of infections across age groups. We added two subscripts to transmission rate μ to create $\mu_{p,q}$: p for the age of an infectious individual, and q for the age of the individual being infected (Figure 4). Epidemic parameters used in population-based compartmental models were also used to model infections across age groups. We used three transmission rates and three removed rates, based on the number of individuals seeking medical attention.

To construct the layer 2 model, we revised Equations (2a) and (2b) to (3a) and (3b), respectively, without making any other changes to the Equation (2) subequations, as follows:

$$\frac{dS_p}{dt} = S_p\chi_p\chi_p(\beta_{2pp}I_{2p} + \beta_{11pp}I_{11p} + \beta_{12pp}I_{12p})/N_p - S_p\sum_{q\neq p}\chi_q\chi_p(\beta_{2qp}I_{2q} + \beta_{11qp}I_{11q} + \beta_{12qp}I_{12q})/N_p \tag{3a}$$

$$\frac{dL_p}{dt} = -\theta_p L_p + S_p\chi_p\chi_p(\beta_{2pp}I_{2p} + \beta_{11pp}I_{11p} + \beta_{12pp}I_{12p})/N_p + S_p\sum_{q\neq p}\chi_q\chi_p(\beta_{2qp}I_{2q} + \beta_{11qp}I_{11q} + \beta_{12qp}I_{12q})/N_p \tag{3b}$$

2.3. Layer 3: Commuting

For the present research we focused on the impacts of daily commuting networks on the spreading of an influenza virus. Since influenza viruses are transmitted via airborne droplets, commuter hosts are capable of

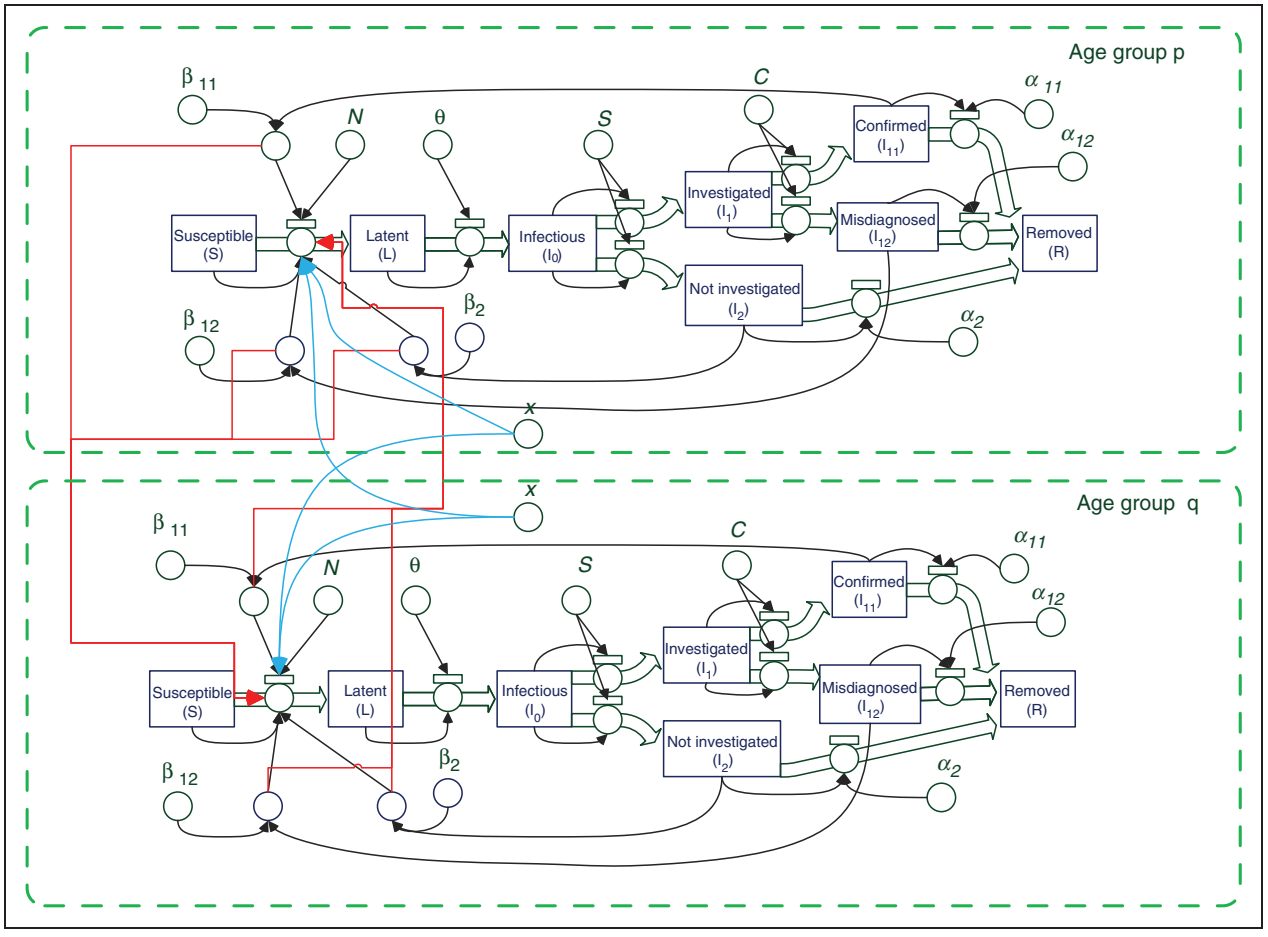

Figure 4. MEDSim layer 2 architecture flowchart. Red lines indicate parameters for other (non-p and non-q) age groups. Blue curves indicate relative percentages of each age group within the total population of each location. (Color online only).

infecting other individuals along their standard routes. The layer 3 model reflects two assumptions regarding hosts with jobs: they commute over longer distances than individuals who stay at home or travel to local centers such as schools, and they tend to come into contact with individuals in the same age group along their routes and at their destinations. We also assumed higher contact frequencies among individuals in more densely populated areas. Accordingly, the layer 3 model considers four features associated with travel between population centers (locations).

$\sigma(p)$, a binary value representing whether age level p is the commuter age level – that is, $\sigma(p) = \begin{cases} 1 & \text{if } p = \text{commutable age level} \\ 0 & \text{otherwise} \end{cases}$. We assumed that children and seniors are less likely than adults to commute on a daily basis, making adults the most likely carriers of pathogens between locations.

$w_{j,i}$, indicating how many individuals commute from location j to location i on a daily basis.

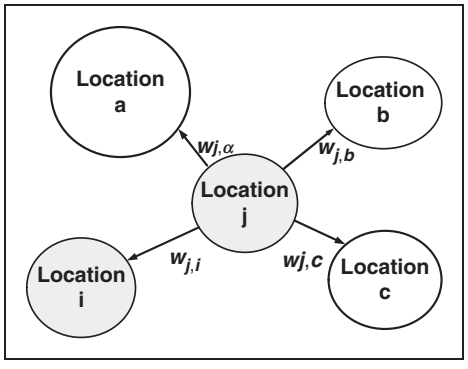

Figure 5. Potential movement of infectivity between locations *i* and *j*.

η^i, a weighting factor representing the average number of contacts among individuals in location i on a daily basis.

d^i, a normalized population density value for location i.

For all i and j locations in a w commuting network, we used the geodemographic weight shown as

Equation (4) to measure the effects of commuting on i and j population interactions:

$$\text{Geodemographic weiht}\ (j,i) = \sigma(p) d^i \eta^i \frac{w_{j,i}}{\sum_{k \neq j} w_{j,k}} \quad (4)$$

As shown in Figure 5, the commuting population age level in this example is adult (15–64). The $\sigma(p)$ function represents whether age group p is a traveling population. For all i locations in the commuting network, the term $N(i)$ represents the set of locations connected to location i within commuting network w. The term $w_{j,i}/\sum_{k \neq j} w_{j,k}$ is the ratio of commuters between locations j and i to commuters between j and all other locations. If location i is a large urban center, $w_{j,i}/\sum_{k \neq j} w_{j,k}$ will be large; if i is a suburb or rural location, it will be small. Public health policies involving transportation can be tested by changing contact rates among population centers in the layer 3 model.

The layer 3 framework is presented in Figure 6. To construct the layer 3 model, we revised Equations (3a) and (3b) to Equations (4a) and (4b), respectively. Note the addition of a geodemographic weight on the third line of each equation. All other Equation (2) subequations are the same.

$$\begin{aligned}\frac{dS_p^i}{dt} = & -S_p^i d^i \chi_p^i \chi_p^i (\beta_{2pp}^i I_{2p}^i + \beta_{11pp}^i I_{11p}^i + \beta_{12pp}^i I_{12p}^i)/N_p^i \\ & - S_p^i \sum_{q \neq p} d^i \chi_q^i \chi_p^i (\beta_{2qp}^i I_{2q}^i + \beta_{11qp}^i I_{11q}^i + \beta_{12qp}^i I_{12q}^i)/N_q^i \\ & - \sum_{j \in N(i)} \sigma(p) d^i \eta^i S_p^i \frac{w_{j,i}}{\sum_{k \neq j} w_{j,k}} \\ & \times (\beta_{2pp}^j I_{2p}^j + \beta_{11pp}^j I_{11p}^j + \beta_{12pp}^j I_{12p}^j)/N_p^j \end{aligned} \quad (4a)$$

$$\begin{aligned}\frac{dL_p^i}{dt} = & -\theta_p^i L_p^i + S_p^i d^i \chi_p^i \chi_p^i (\beta_{2pp}^i I_{2p}^i + \beta_{11pp}^i I_{11p}^i + \beta_{12pp}^i I_{12p}^i)/N_p^i \\ & + S_p^i \sum_{q \neq p} d^i \chi_q^i \chi_p^i (\beta_{2qp}^i I_{2q}^i + \beta_{11qp}^i I_{11q}^i + \beta_{12qp}^i I_{12q}^i)/N_q^i \\ & + \sum_{j \in N(i)} \sigma(p) d^i \eta^i S_p^i \frac{w_{j,i}}{\sum_{k \neq j} w_{j,k}} \\ & \times (\beta_{2pp}^j I_{2p}^j + \beta_{11pp}^j I_{11p}^j + \beta_{12pp}^j I_{12p}^j)/N_p^j \end{aligned} \quad (4b)$$

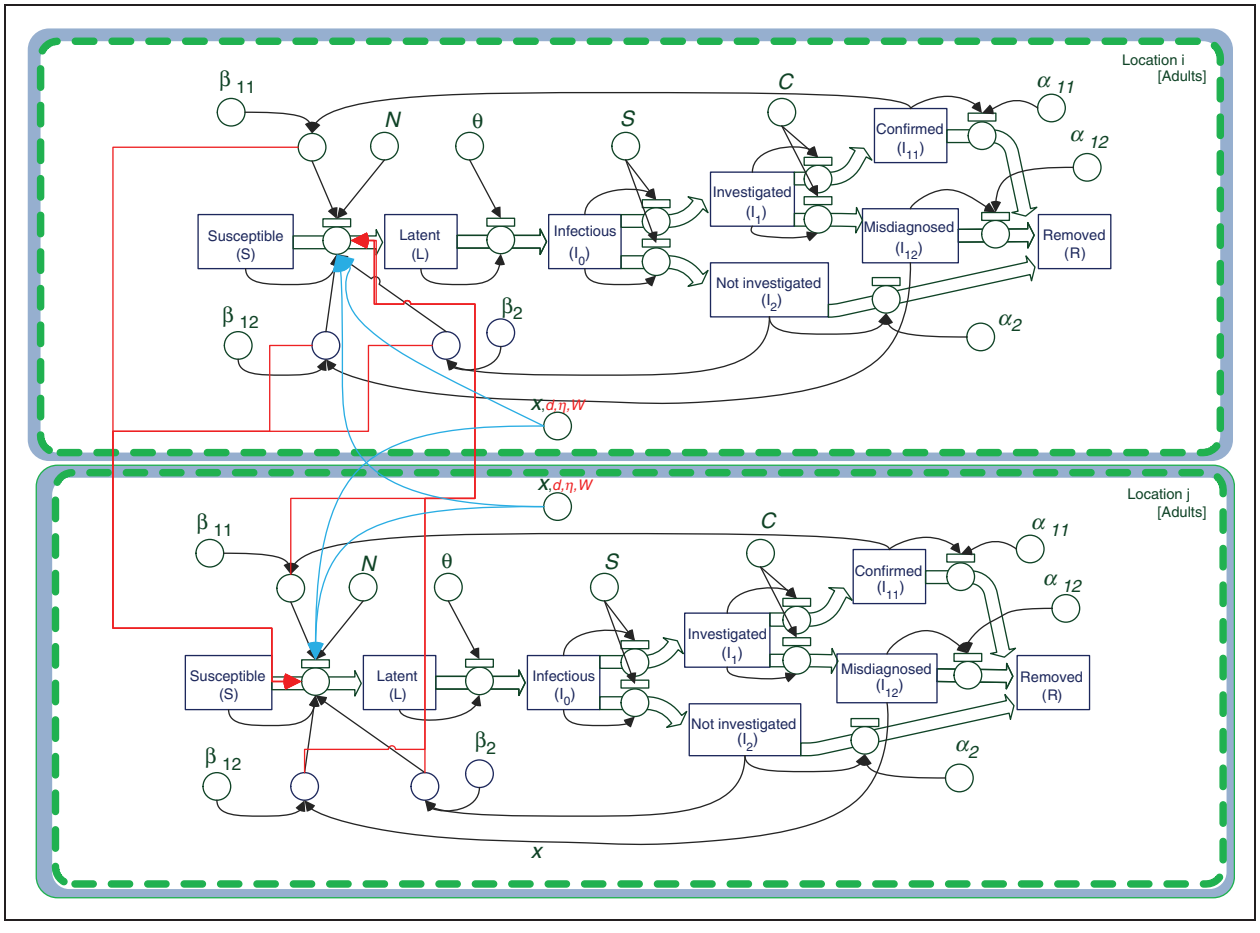

Figure 6. MEDSim layer 3 architecture flowchart. Properties associated with commuting between two locations are indicated by red lines. Additional location properties are indicated by blue lines. (Color online only).

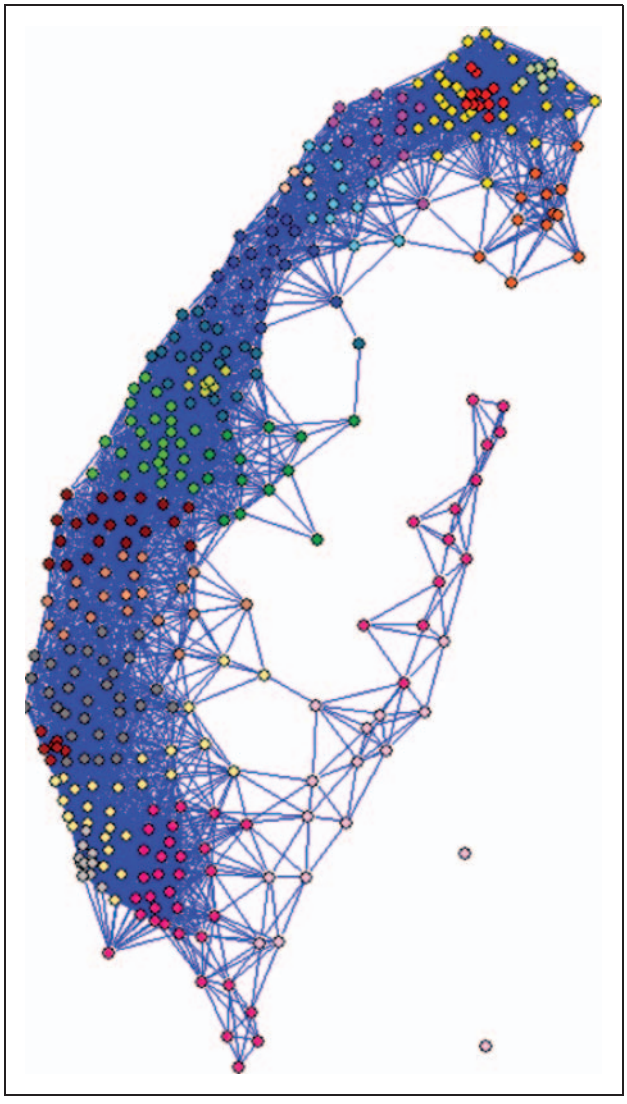

Figure 7. Taiwan's nationwide commuting network.

2.4. Layer 4: Nationwide interactions

We used Taiwan's national travel network and commuting weight $w_{j,i}$ to simulate individual movement within regions (layer 3). Nodes represent locations, and edges represent commuting weights between locations. Once transportation data are obtained, nodes can represent any scale – for instance, a building for city simulations and a town for regional or national simulations. In the present study, each node represents an individual town. Layer 4 of our model consists of 409 towns and 19,014 links (Figure 7) representing Taiwan's national commuting network, which can be manipulated to determine the effects of various movement policies and commuting restrictions.

After combining the four layers, the complete MEDSim model can be expressed as

$$\begin{aligned}\frac{dS_p^i}{dt} = & -S_p^i d^i \chi_p^i \chi_p^i (\beta_{2pp}^i I_{2p}^i + \beta_{11pp}^i I_{11p}^i + \beta_{12pp}^i I_{12p}^i)/N_p^i \\ & - S_p^i \sum_{q \neq p} d^i \chi_q^i \chi_p^i (\beta_{2qp}^i I_{2q}^i + \beta_{11qp}^i I_{11q}^i + \beta_{12qp}^i I_{12q}^i)/N_q^i \\ & - \sigma(p) d^i \eta^i S_p^i \sum_{j \in N(i)} \frac{w_{j,i}}{\sum_{k \neq j} w_{j,k}} \\ & \times (\beta_{2pp}^j I_{2p}^j + \beta_{11pp}^j I_{11p}^j + \beta_{12pp}^j I_{12p}^j)/N_p^j \end{aligned} \tag{5a}$$

$$\begin{aligned}\frac{dL_p^i}{dt} = & -\theta_p^i L_p^i + S_p^i d^i \chi_p^i \chi_p^i \left(\beta_{2pp}^i I_{2p}^i + \beta_{11pp}^i I_{11p}^i + \beta_{12pp}^i I_{12p}^i\right)/N_p^i \\ & + S_p^i \sum_{q \neq p} d^i \chi_q^i \chi_p^i \left(\beta_{2qp}^i I_{2q}^i + \beta_{11qp}^i I_{11q}^i + \beta_{12qp}^i I_{12q}^i\right)/N_q^i \\ & + \sigma(p) d^i \eta^i S_p^i \sum_{j \in N(i)} \frac{w_{j,i}}{\sum_{k \neq j} w_{j,k}} \\ & \times (\beta_{2pp}^j I_{2p}^j + \beta_{11pp}^j I_{11p}^j + \beta_{12pp}^j I_{12p}^j)/N_p^j \end{aligned} \tag{5b}$$

$$\frac{dI_{0p}^i}{dt} = -I_{0p}^i + \theta_p^i L_p^i \tag{5c}$$

$$\frac{dI_{1p}^i}{dt} = -I_{1p}^i (t - T) + s_p^i I_{0p}^i \tag{5d}$$

$$\frac{dI_{2p}^i}{dt} = -\alpha_{2p}^i I_{2p}^i + (1 - s_p^i) I_{0p}^i \tag{5e}$$

$$\frac{dI_{11p}^i}{dt} = -\alpha_{11p}^i I_{11p}^i + c_p^i I_{1p}^i (t - T) \tag{5f}$$

$$\frac{dI_{12p}^i}{dt} = -\alpha_{12p}^i I_{12p}^i + (1 - c_p^i) I_{1p}^i (t - T) \tag{5g}$$

$$\frac{dR_p^i}{dt} = \alpha_{11p}^i I_{11p}^i + \alpha_{12p}^i I_{12p}^i + \alpha_{2p}^i I_{2p}^i \tag{5h}$$

The parameters used in Equation (5) are listed in Table 1.

2.5. Technological framework

Figure 8 shows the MEDSim technological framework, including a simulation flowchart, census databases, and relationships between the four MEDSim layers and the databases. The first step is to manually create an Excel data set for the scenario in question – for example, determining breakout locations or public health policies. Most data sets consist of spatial locations and census information, which are used to establish geographic and demographic categories; each MEDSim parameter belongs to at least one of the two.

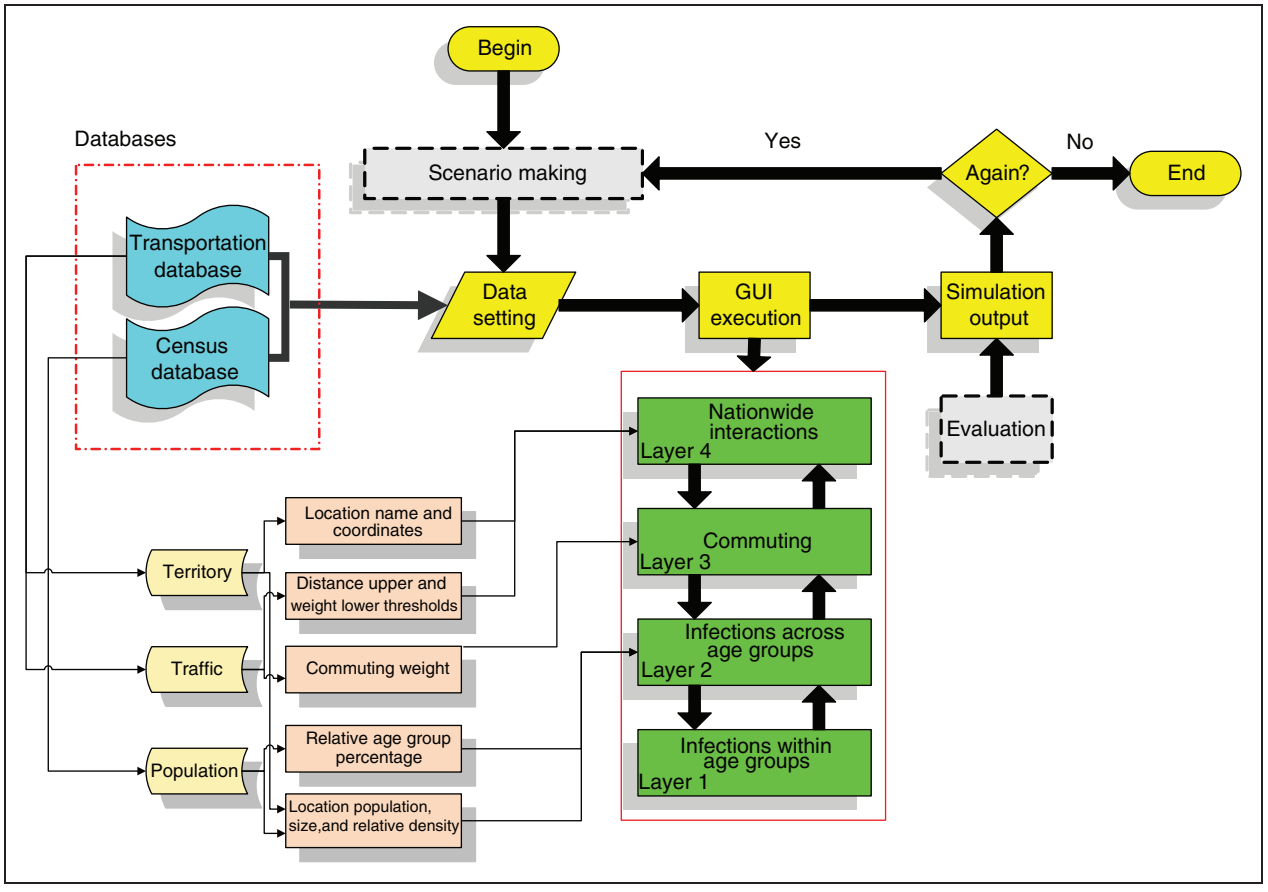

Figure 8. MEDSim simulation tool framework.

Since our layer 1 focus in this example is on disease progression at an individual level, standard expert-based parameters in compartmental models associated with epidemics were used instead of transportation or census databases.[16] In layer 2, percentages of individuals in each age group were determined from census data, and the numbers of individuals in each location were gathered from transportation databases. In layer 3, transportation databases were used to gather information on the numbers of individuals traveling between towns on a daily basis. In layer 4, transportation data were used to establish the underlying national travel network.

Figure 9 presents a screenshot of a MEDSim graphical user interface (GUI). Multilayer epidemic model parameters are initialized at the beginning of each simulation. Model parameters requiring setup are: (a) initial outbreak conditions, including the name of the town and number of infected persons in an age group identified by the surveillance system; (b) disease transmission parameters at different layers, including transmission, latent, and removed rates according to the SLIR process for each age group, contact rates between age groups, and regional contact probabilities between towns; and (c) output maps and charts for the towns of interest and severity indicators to be monitored (e.g. daily infected cases, daily new cases, and epidemic velocity and acceleration). Daily epidemic progress can be monitored in terms of sizes and locations of red dots on maps (infected individuals), epidemic curves on time charts, and output panels (numbers of infected individuals at different times in different locations). Regarding kernel execution, MEDSim models can be used for computing epidemic dynamics. Simulation results can be shown as graphical curves or expressed and recorded as numerical files. Lastly, simulation results are evaluated by users, who can repeat steps as required.

2.6. Statistical analysis for parameterization

To test the reliability and validity of time-series MEDSim data, we used two indices to compare simulated and actual numbers of infected individuals: correlation coefficient (CC) and coefficient of efficiency (CE), respectively expressed as Equations (6)

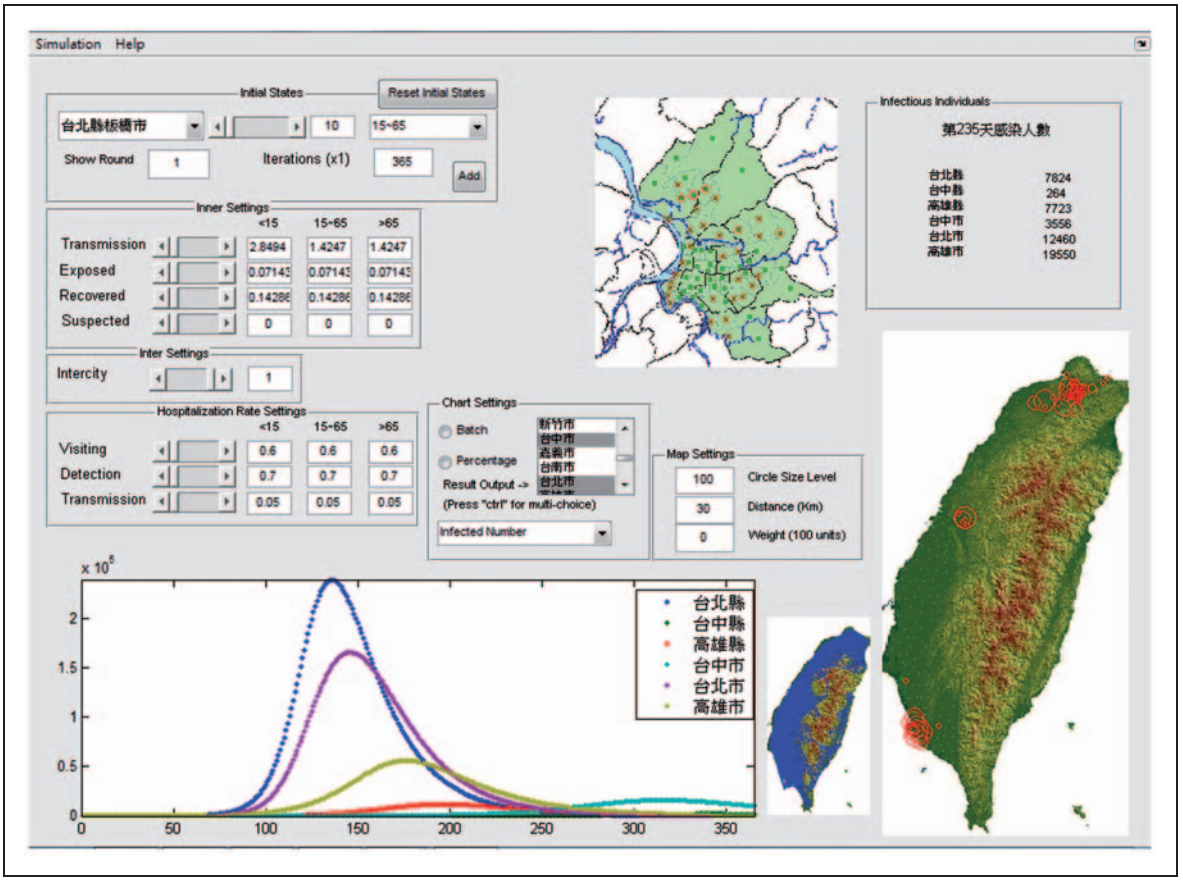

Figure 9. MEDSim implementation GUI.

and (7).[22] Here $\{X_t|t = 1, 2, \ldots, n\}$ represents the number of actual infected individuals and $\{Y_t|t = 1, 2, \ldots, n\}$ the number calculated by the MEDSim. In both sets, t denotes the time step (in 1 week units); a total of n weeks is represented by each set. We use $\overline{X}$ and $\overline{Y}$ to denote the means of X_t and Y_t, respectively. The CC test measures data distance: higher positive values indicate positive correlations and lower negative values indicate negative correlations. The CE test is used to measure the level of accuracy between two data sets; higher values indicate greater accuracy:

$$CC = \frac{\sum_{t=1}^{n}(X_t - \overline{X})(Y_t - \overline{Y})}{\sqrt{\sum_{t=1}^{n}(X_t - \overline{X})^2}\sqrt{\sum_{t=1}^{n}(Y_t - \overline{Y})^2}} \in [-1, 1] \quad (6)$$

$$CE = 1 - \left[\frac{\sqrt{\sum_{t=1}^{n}(X_t - Y_t)^2}}{\sqrt{\sum_{t=1}^{n}(X_t - \overline{X})^2}}\right] \in [0, 1] \quad (7)$$

3. Results and discussion

We tested MEDSim reliability (in terms of parameter calibration and model fit) with actual epidemic curves, tested and compared public health policies based on the above parameters, and used MEDSim to simulate the influenza A (H1N1) virus and to determine the effects of the chosen policies. To establish simulation parameter settings, we used population data from the Republic of China (ROC) Ministry of the Interior and transportation data from the ROC Transportation Institute.[38]

3.1. Parameterization

We used the seasonal influenza A and swine-origin influenza A (H1N1) viruses to perform parameterization. The default parameter values are shown in Table 1. We systematically calibrated parameters for both viruses to create a small range, based on parameters normally used with standard SLIR settings.[16] Summaries of MEDSim attribute settings and values are given in Tables 2 and 3. The transmission rates β^i_{11pp}, β^i_{12pp}, and β^i_{2pp} were directional between age groups. Individual age group targets are presented in

Table 2. MEDSim parameters used for fitting simulation curves with actual seasonal influenza A curves in Taiwan between September 2008 and April 2009

		Value					
Layer	Attribute	Children		Adults		Seniors	
1	β^i_{11pp}	1.3333		0.6667		0.6667	
	β^i_{12pp}	3.3333		1.6667		1.6667	
	β^i_{2pp}	3.3333		1.6667		1.6667	
	θ^i_p			0.0714			
	α^i_{11p}			0.1429			
	α^i_{12p}			0.2500			
	α^i_{2p}			0.1429			
	Target	Adults	Seniors	Children	Seniors	Children	Adults
2	β^i_{11xy}	0.6667	0.6667	1.3333	0.6667	1.3333	0.6667
	β^i_{12xy}	1.6667	1.6667	3.3333	1.6667	3.3333	1.6667
	β^i_{2xy}	1.6667	1.6667	3.3333	1.6667	3.3333	1.6667

Table 3. MEDSim parameters used for fitting simulation curves to actual swine-origin influenza A (H1N1) curves in Taiwan from week 25 to week 52

		Value					
Layer	Attribute	Children		Adults		Seniors	
1	β^i_{11pp}	2.6667		1.3333		1.3333	
	β^i_{12pp}	3.3333		1.6667		1.6667	
	β^i_{2pp}	3.3333		1.6667		1.6667	
	θ^i_p			0.0714			
	α^i_{11p}			0.3333			
	α^i_{12p}			0.1429			
	α^i_{2p}			0.1667			
	Target	Adults	Seniors	Children	Seniors	Children	Adults
2	β^i_{11xy}	1.3333	1.3333	2.6667	1.3333	2.6667	1.3333
	β^i_{12xy}	1.6667	1.6667	3.3333	1.6667	3.3333	1.6667
	β^i_{2xy}	1.6667	1.6667	3.3333	1.6667	3.3333	1.6667

the form of sub-columns. Experimental results from applying the MEDSim using the Table 2 and 3 parameter values for the two influenza viruses are shown in Figures 10(a) and (b), respectively. Actual and simulated case data for both influenzas are shown in weekly units.

Our CC and CE results for the two influenza epidemics are 0.86 and 0.74 for seasonal and 0.77 and 0.36 for swine-origin H1N1. In Figure 10(a) we plotted the fractions of new infected cases of seasonal influenza A in Taiwan between September 2008 and April 2009, normalized to total cases. Higher CC and CE values for seasonal influenza explain the similarities between the two curves. In Figure 10(b) we plotted fractions of new infected cases for the swine-origin influenza A virus in Taiwan from week 25 to week 52 in 2009, also normalized to total cases. As shown, the number of actual cases decreased between weeks 37 and 48, followed by an increasing trend, resulting in a lower CE value. This two-wave pattern is very similar to global diffusion patterns associated with international travel. Because we did not incorporate international travel at this stage, our swine-origin H1N1 model failed to capture the second wave; however, it did capture the peak time for the first (primary) wave (Figure 10(b)).

3.2. Intervention policy evaluation

We tested and compared different public health policies using the above-described parameters, simulated the

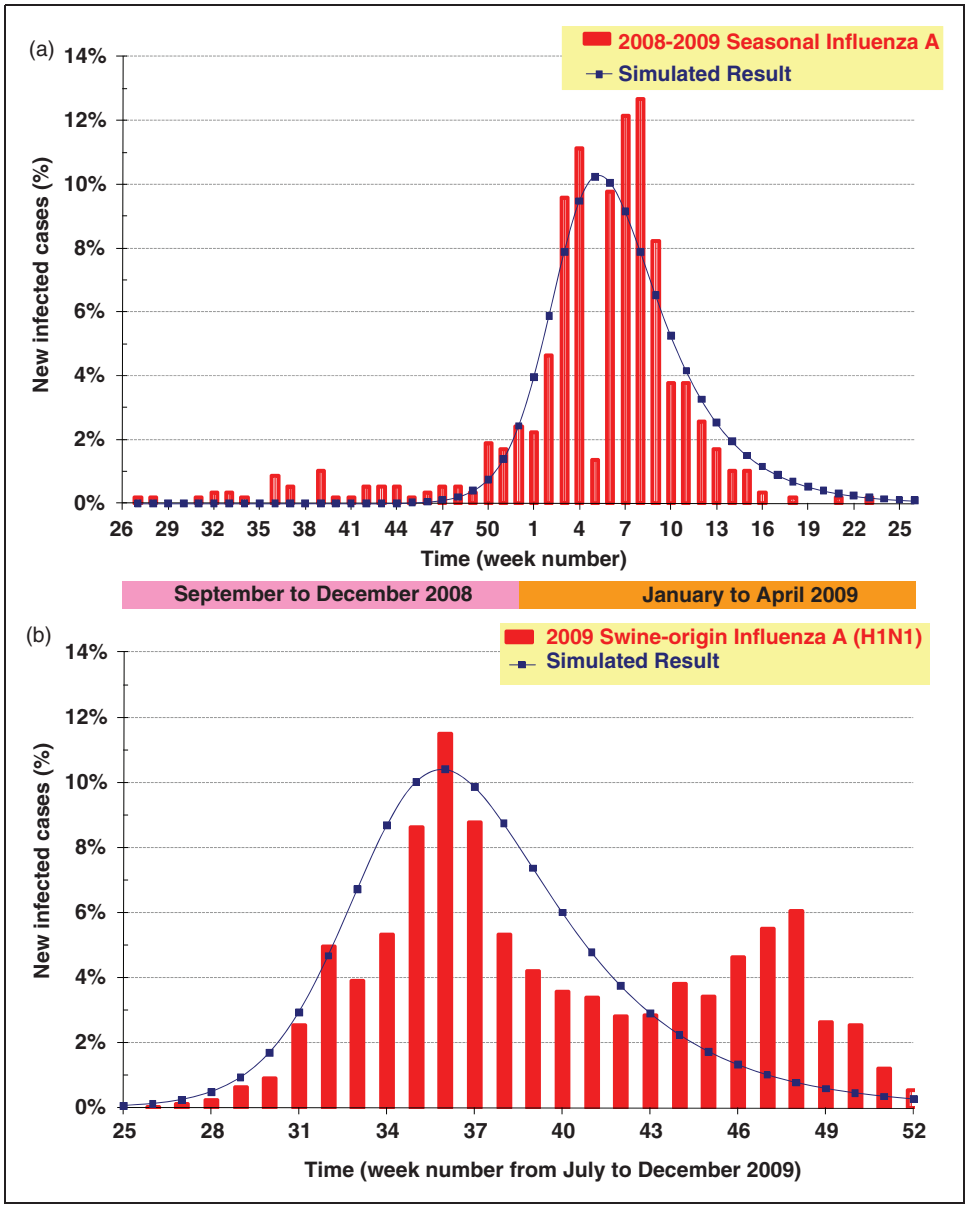

Figure 10. Comparison of weekly new infected cases between actual and simulated results normalized for (a) seasonal influenza A and (b) swine-origin H1N1 influenza A.

Table 4. Observation index values according to different transmission rates

	Transmission rate reduction (%)				
Observation index	0%	30%	50%	70%	90%
Total cases.	1,784,044	1,407,752	1,108,520	485,761	8
New infected cases at epidemic curve peak	171,329	113,898	64,926	12,231	8
Week number of epidemic curve peak	20	26	36	77	∞
Percentage of new infected cases at epidemic curve peak	9.6%	6.4%	3.6%	0.7%	0%
$\left(\frac{\text{Total cases of epidemic curve}}{\text{Total cases of basic epidemic curve}}\right)$	100%	78.9%	62.1%	27.2%	0.%

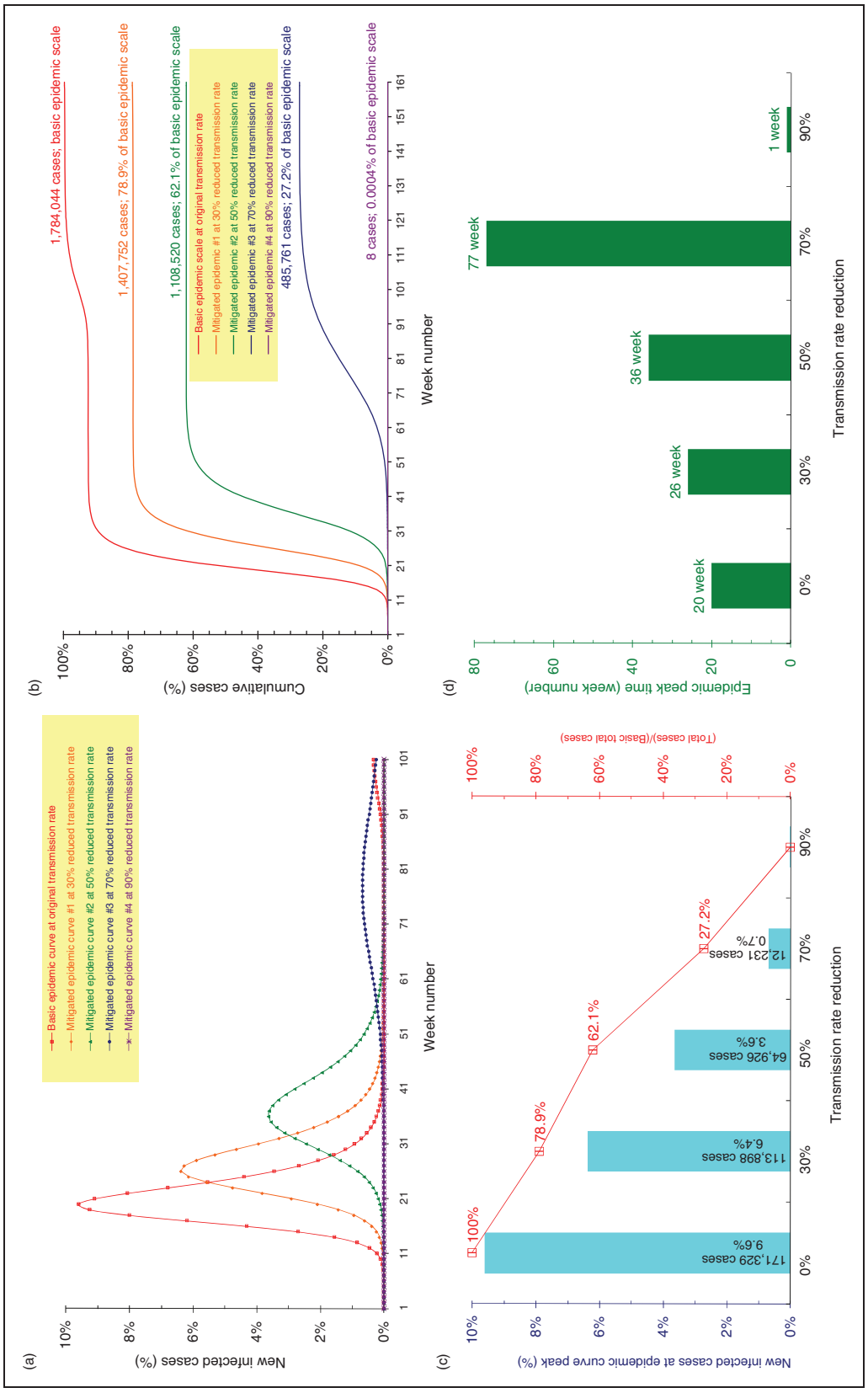

Figure 11. (a) New infected cases per week at different transmission rates. (b) Cumulative new infected cases at different transmission rates. (c) Basic epidemic curve at a 0% reduced transmission rate expressed according to two observation indexes. (d) Comparison of new infected cases at epidemic curve peak at different transmission rates. (e) Weekly new cases at curve peak at different transmission rates. (f) New infected cases at epidemic curve peak according to various intervention policy scenarios. (g) Numbers of infected cases according to various intervention policy scenarios. (h) Week numbers of epidemic curve peaks according to various intervention policy scenarios. (Color online only).

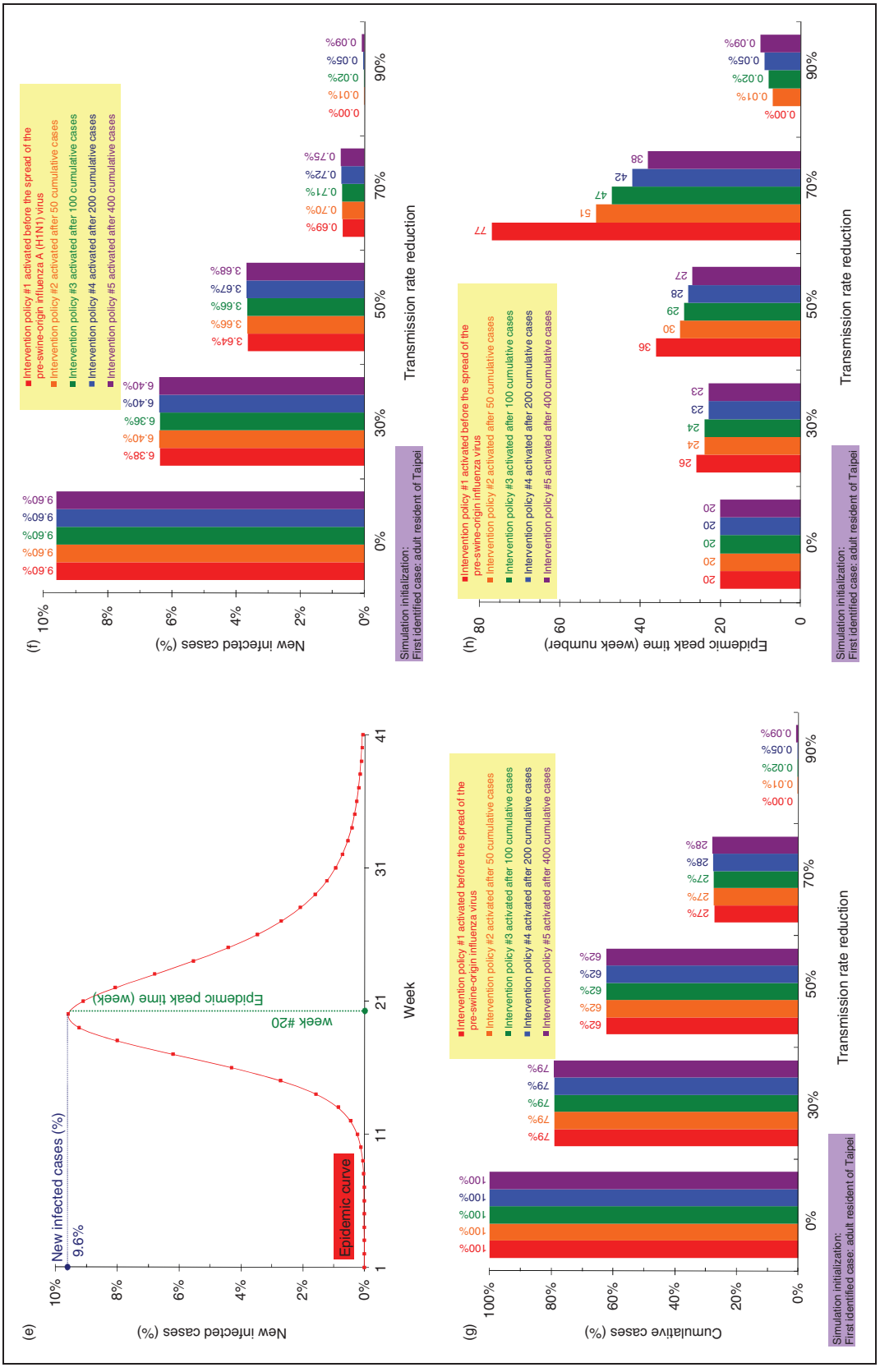

Figure 11. Continued.

effects of medical advice quality and number of commuters, and compared original epidemic curves with those following public health policy implementation. Special emphases were placed on peak numbers of infected cases and peak infection days. The goals of public health officials include reducing the peak number (since it has a direct effect on social costs, such as drugs and hospital beds) and delaying peak day.

Figure 11 has two parts, one addressing the impacts of transmission rate reduction and one the effects of various intervention policies. The results from simulated observation indices for different transmission rates are shown in Table 4. According to the Figure 11(a) data for weekly fractions of new infected cases, both curve peak and height were negatively affected by decreased transmission rate. According to the Figure 11(b) data on the cumulative number of new infections at different transmission rates, that number decreased as transmission rate decreased. In Figure 11(c) we used two observation indices to distinguish between the epidemic curve produced by the highest transmission rate and the curves shown in Figure 11(a). According to the first observation index (fraction of new infected cases at epidemic curve peak), the strongest epidemic disease transmission intensity affects a population and negatively impacts public health resources over a period of one week. The second index (epidemic curve peak week number) indicates the severity and urgency of an epidemic, thus impacting deadlines for initiating public health policies; higher values indicate more time for making policy decisions.

The results from our comparisons of epidemic curve peaks at different reduced transmission rates are shown in Figure 11(c). The basic fraction of new infected cases at curve peak (noted as 100%, with a transmission rate of 1.0) is shown in the leftmost part of the graph. The relative total number of cases (red line) consists of two line segments, one from 1.0 to 0.5 and the other from 0.5 to 0.1. According to this result, transmission rate should be reduced by at least 50% to obtain better peak number suppression. An obvious decrease in peak number occurs when the transmission rate reduction is 70%.

Curve peak week numbers at different transmission rates are shown in Figure 11(d). Note that week number increased as transmission rate decreased – a positive result for public health policy makers. The results from simulations of various long- and short-term intervention policy activation scenarios are shown in Figures 11(f)–(h). No differences in numbers of infected cases were observed for different intervention policy activation times (Figures 11(f) and (g)). However, epidemic peak was delayed from weeks 55 to 71 when intervention policy activation time was set at 50 with a 70% reduction in transmission rate (Figure 11(h)). Activation time exerted a much weaker effect on peak timing at a 30% reduction in transmission rate. According to these results, while time of intervention policy activation did not significantly reduce the number of infected cases, it did exert an obvious effect in terms of delaying peak time – a positive result for public health policy determination and preparation.

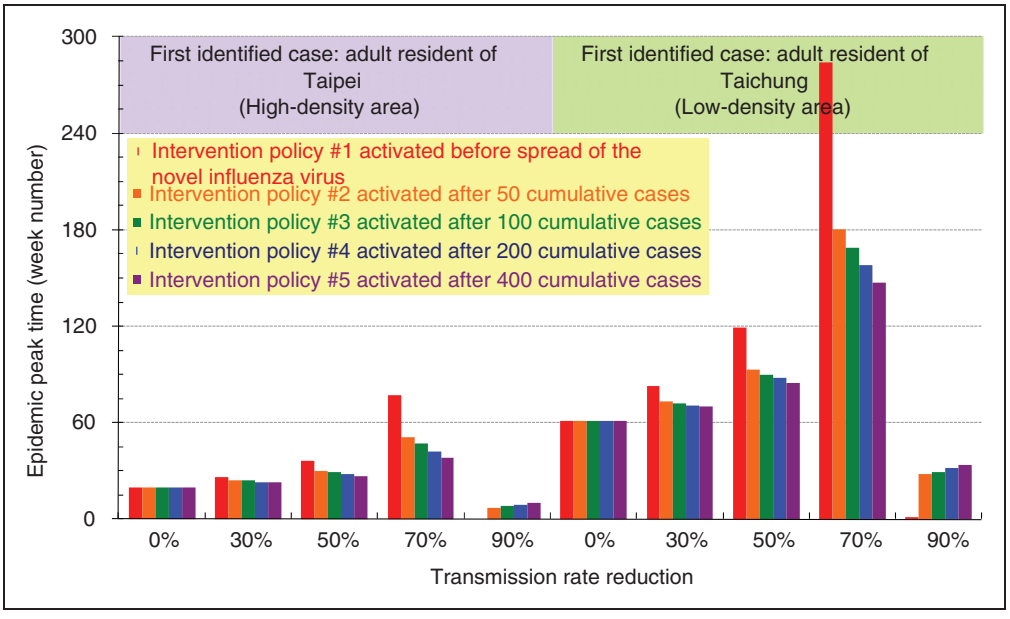

Figure 12. Epidemic peak week numbers for urban and rural areas.

Table 5. Observation index values according to different policy activation scenarios during swine-origin H1N1 influenza A outbreak in Taipei

		Transmission rate reduction				
Policy activation time	Observation index	0%	30%	50%	70%	90%
Scenario #1 Pre-virus appearance	Total cases	1,784,044	1,407,752	1,108,520	485,761	8
	New infected cases at epidemic curve peak	171,329	113,898	64,926	12,231	8
	Week number of epidemic curve peak	20	26	36	77	0
	Percentage of new infected cases at epidemic curve peak	9.60%	6.38%	3.64%	0.69%	0%
	$\left(\frac{\text{Total cases of epidemic curve}}{\text{Total cases of basic epidemic curve}}\right)$	100%	78.90%	62.14%	27.23%	0.00%
Scenario #2 After 50 cases are diagnosed	Total cases	Same as above	1,409,827	1,108,794	487,425	855
	New infected cases at epidemic curve peak		114,120	65,235	12,468	155
	Week number of epidemic curve peak		24	30	51	7
	Percentage of new infected cases at epidemic curve peak		6.40%	3.66%	0.70%	0%
	$\left(\frac{\text{Total cases of epidemic curve}}{\text{Total cases of basic epidemic curve}}\right)$		79.02%	62.15%	27.32%	0.05%
Scenario #3 After 100 cases are diagnosed	Total cases	Same as above	1,410,263	1,108,993	488,900	1,991
	New infected cases at epidemic curve peak		113,532	65,314	12,604	349
	Week number of epidemic curve peak		24	29	47	8
	Percentage of new infected cases at epidemic curve peak		6.36%	3.66%	0.71%	0%
	$\left(\frac{\text{Total cases of epidemic curve}}{\text{Total cases of basic epidemic curve}}\right)$		79.05%	62.16%	27.40%	0.11%
Scenario #4 After 200 cases are diagnosed	Total cases	Same as above	1,410,782	1,109,355	491,563	4,599
	New infected cases at epidemic curve peak		114,191	65,442	12,883	818
	Week number of epidemic curve peak		23	28	42	9
	Percentage of new infected cases at epidemic curve peak		6.40%	3.67%	0.72%	0%
	$\left(\frac{\text{Total cases of epidemic curve}}{\text{Total cases of basic epidemic curve}}\right)$		79.08%	62.18%	27.55%	0.26%
Scenario #5 After 400 cases are diagnosed	Total cases	Same as above	1,411,273	1,109,893	496,246	10,000
	New infected cases at epidemic curve peak		114,185	65,669	13,408	1,680
	Week number of epidemic curve peak		23	27	38	10
	Percentage of new infected cases at epidemic curve peak		6.40%	3.68%	0.75%	0%
	$\left(\frac{\text{Total cases of epidemic curve}}{\text{Total cases of basic epidemic curve}}\right)$		79.11%	62.21%	27.82%	0.56%

Next, we compared differences in swine-origin H1N1 influenza A starting locations in Taiwan and their effects on the subsequent spreading of the disease (Figure 12, Tables 5 and 6). Taipei was labeled a high-density area and Taichung a low-density area. In the first (pre-swine-origin virus) scenario, case numbers peaked much earlier in Taipei (20) than in Taichung (61). When the transmission rate was reduced to 30%, the Taichung peak was significantly delayed. When comparing numbers of infected cases at the curve peak, both locations had approximately the same number of new cases, but Taipei had a much larger number of total cases. After reducing the transmission rate from 50% to 30%, Taichung had a much later peak week compared to Taipei, with no effect of intervention policy activation time on the total number of cases or newly infected cases in either location. The results suggest that less densely populated starting locations are more sensitive to intervention policy activation time – that is, the combination of early activation time and low transmission rate significantly delays epidemic curve peaks in less densely populated locations.

Table 6. Observation index values according to different policy activation scenarios during swine-origin H1N1 influenza A outbreak in Taichung

		Transmission rate reduction				
Policy activation time	Observation index	0%	30%	50%	70%	90%
Scenario #1 Before the swine-origin influenza A (H1N1) virus emerges	Total cases	2,190,247	1,672,733	1,112,428	485,801	8
	New infected cases at epidemic curve peak	172,083	114,556	64,551	12,186	8
	Week number of epidemic curve peak	61	83	119	284	1
	Percentage of new infected cases at epidemic curve peak	7.86%	5.23%	2.95%	0.56%	0%
	$\left(\frac{\text{Total cases of epidemic curve}}{\text{Total cases of basic epidemic curve}}\right)$	100%	76.37%	50.79%	22.18%	0.00%
Scenario #2 After 50 cumulative swine-origin influenza A (H1N1) infected cases are diagnosed	Total cases	(see above)	1,672,266	1,117,265	487,030	767
	New infected cases at epidemic curve peak		113,760	64,598	12,200	120
	Week number of epidemic curve peak		73	93	180	28
	Percentage of new infected cases at epidemic curve peak		5.19%	2.95%	0.56%	0%
	$\left(\frac{\text{Total cases of epidemic curve}}{\text{Total cases of basic epidemic curve}}\right)$		76.35%	51.01%	22.24%	0.04%
Scenario #3 After 100 cumulative swine-origin influenza A (H1N1) infected cases are diagnosed	Total cases	(see above)	1,671,019	1,120,702	488,492	1,723
	New infected cases at epidemic curve peak		113,672	64,430	12,194	273
	Week number of epidemic curve peak		72	90	169	29
	Percentage of new infected cases at epidemic curve peak		5.19%	2.94%	0.56%	0%
	$\left(\frac{\text{Total cases of epidemic curve}}{\text{Total cases of basic epidemic curve}}\right)$		76.29%	51.17%	22.30%	0.08%
Scenario #4 After 200 cumulative swine-origin influenza A (H1N1) infected cases are diagnosed	Total cases	(see above)	1,674,627	1,125,289	491,418	3,668
	New infected cases at epidemic curve peak		113,592	64,556	12,198	520
	Week number of epidemic curve peak		71	88	158	32
	Percentage of new infected cases at epidemic curve peak		5.19%	2.95%	0.56%	0%
	$\left(\frac{\text{Total cases of epidemic curve}}{\text{Total cases of basic epidemic curve}}\right)$		76.46%	51.38%	22.44%	0.17%
Scenario #5 After 400 cumulative swine-origin influenza A (H1N1) infected cases are diagnosed	Total cases	(see above)	1,677,338	1,132,127	49,486	7,424
	New infected cases at epidemic curve peak		112,155	64,605	12,188	1057
	Week number of epidemic curve peak		70	85	147	34
	Percentage of new infected cases at epidemic curve peak		5.12%	2.95%	0.56%	0%
	$\left(\frac{\text{Total cases of epidemic curve}}{\text{Total cases of basic epidemic curve}}\right)$		76.58%	51.69%	22.67%	0.34%

4. Conclusion

Our goal in this paper was to integrate complex human travel networks into a standard SLIR disease transmission model to create a four-layer simulation prototype named the MEDSim. The framework is offered to researchers interested in determining the contributions of complex human contact structures to the transmission dynamics of influenza viruses. Our proposed model is capable of providing insights that reflect the dynamic processes of epidemics according to various intervention scenarios involving outbreak location, intervention timing, and different policy suites. We view this multilayer approach as both convenient and effective for public health practitioners and administrators responsible for initiating early responses to potential pandemics, and for assessing intervention strategies in outbreak locations.

This study has several limitations, such as the lack of confirmed numbers of H1N1 influenza A cases in

Taiwan (at this time it is not a notifiable disease in this country). The data used for parameterization reflect severe and hospitalized cases, which we assume as having the same proportions as non-severe cases per time unit. Differences between actual and simulated cases can be significantly reduced when using appropriate parameter values in terms of investigation and detection proportions. Secondly, since the SLIR model is imprecise in terms of its *Removed* designation, we could not address the number of H1N1-related deaths in our discussion of peak time delay. In real-world scenarios involving pandemic diseases with high death rates, peak time delays are very important for disease prevention policy decisions. Thirdly, due to the limited scope of this study, we did not gather and organize the exceptionally large amounts of available data for all areas represented by network nodes (e.g. workplaces, houses, and schools) or network data for long-distance transportation (e.g. highway, railway, or airline). Instead, we used location and age for population grouping, based on their similarities in responses to epidemic-related factors. Furthermore, we did not address other individual attributes, such as income level or number of social groups per individual, when determining transmission rate, removed rate, or other parameters.

We believe our proposed MEDSim framework can help public health organizations decide when to implement intervention strategies by simultaneously analyzing multilayer interactions. To build on this positive beginning, we plan to expand the multilayer framework to make it suitable for other acute diseases, as well as to make it responsive to complex human contact structures. Although our focus in this pilot study was on a novel influenza epidemic in Taiwan, the general multilayer framework concepts can be transferred to other sites. The SLIR model in layer 1 can be considered a general model for all droplet-transmitted respiratory infections, and the age group and commuting interactions in layers 2 and 3 can be disassembled to meet the requirements of risk factors for other infectious diseases. Furthermore, the network topology in layer 4 can be modified to meet the needs of different scales of link-node structures as noted in an earlier section. However, when transferring the proposed multilayer framework to other sites, data on the link-node network structures and transmission parameters for the diseases being studied must be collected, organized, and verified. One of our goals is to establish a portable framework for this procedure. Our plans also include extending the MEDSim for use as a general-purpose disease modeling framework. For example, we will work on adding long-distance transportation networks to our model to determine the impacts of shutting down railway or airline systems, and on modifying different contact structures (e.g. mosquito–human) to model vector-borne diseases, such as dengue fever and malaria, as well as human–animal contact diseases, such as rabies and Japanese encephalitis.

Funding

This research was supported by a grant from the ROC National Science Council (NSC 98-2410-H-002-168-MY2 and NSC 98-2314-B-182-043). The authors are also grateful for financial support provided by the Infectious Disease Research and Education Center at National Taiwan University and Department of Health, Executive Yuan, ROC (Taiwan). The funders had no role in study design, data collection and analysis, or preparation of the manuscript.

Conflict of interest statement

The Authors declare no conflict of interest related to this work.

References

1. Smith GJ, Vijaykrishna D, Bahl J, Lycett SJ, Worobey M, Pybus OG, et al. Origins and evolutionary genomics of the 2009 swine-origin H1N1 influenza A epidemic. *Nature* 2009; 459: 1122–1125.
2. Feng Z, Huang W and Castillo-Chavez C. Global behavior of a multi-group SIS epidemic model with age structure. *J Differ Equat* 2005; 218: 292–324.
3. Inaba H. Age-structured homogeneous epidemic systems with application to the MSEIR epidemic model. *J Math Biol* 2007; 54: 101–146.
4. Langlais M and Naulin JM. An age structured SI epidemic problem in a heterogeneous environment. *Evol Equat Appl Phys Ind Life Sci Econ* 2003; 55: 307–321.
5. Shim E, Feng Z, Martcheva M and Castillo-Chavez C. An age-structured epidemic model of rotavirus with vaccination. *J Math Biol* 2006; 53: 719–746.
6. Supriatna AK, Soewono E and Van Gils SA. A two-age-classes dengue transmission model. *Math Biosci* 2008; 216: 114–121.
7. Wang W and Zhao XQ. An age-structured epidemic model in a patchy environment. *SIAM J Appl Math* 2005; 65: 1597–1614.
8. Yang Y, Sugimoto JD, Halloran ME, Basta NE, Chao DL, Matrajt L, et al. The transmissibility and control of pandemic influenza A (H1N1) virus. *Science* 2009; 326: 729–733. doi:10.1126/science.1177373.
9. Fraser C, Donnelly CA, Cauchemez S, Hanage WP, Van Kerkhove MD, Hollingsworth TD, et al. Pandemic potential of a strain of influenza A (H1N1): Early findings. *Science* 2009; 324: 1557–1561.
10. Belshe RB, Swierkosz EM, Anderson EL, Newman FK, Nugent SL and Maassab HF. Immunization of infants and young children with live attenuated trivalent cold-recombinant influenza A H1N1, H3N2, and B vaccine. *J Infect Dis* 1992; 165: 727–732.
11. Marsh RM. *The great transformation: social change in Taipei, Taiwan since the 1960s*. New York: M.E. Sharpe, 1996.

12. González MC, Hidalgo CA and Barabási AL. Understanding individual human mobility patterns. *Nature* 2008; 453: 779.
13. Huang CY, Sun CT, Hsieh JL, Chen YMA and Lin H. A novel small-world model: Using social mirror identities for epidemic simulations. *Simulation* 2005; 81: 671–699.
14. Tomlinson B and Cockram C. SARS: experience at Prince of Wales Hospital, Hong Kong. *The Lancet* 2003; 361: 1486–1487.
15. Riley S. Large-scale spatial-transmission models of infectious disease. *Science* 2007; 316: 1298–1301.
16. Keeling MJ and Rohani P. *Modeling infectious diseases in humans and animals*, 1st edn. New Jersey: Princeton University Press, 2007.
17. Epstein JM. Modeling to contain pandemics. *Nature* 2009; 460: 687, doi:10.1038/460687a.
18. Liu X, Takeuchi Y and Iwami S. SVIR epidemic models with vaccination strategies. *J Theor Biol* 2008; 253(1): 1–11.
19. Pastor-Satorras R and Vespignani A. Immunization of complex networks. *Phys Rev E* 2002; 65: 036104.
20. Li G and Jin Z. Global stability of a SEIR epidemic model with infectious force in latent, infected and immune period. *Chaos Solitons Fractals* 2005; 25: 1177–1184.
21. Boguna M and Pastor-Satorras R. Epidemic spreading in correlated complex networks. *Phys Rev E* 2002; 66: 47104.
22. Huang CY, Sun CT, Hsieh JL and Lin H. Simulating SARS: small-world epidemiological modeling and public health policy assessments. *J Artif Soc Soc Simulat* 2004; 7: http://jasss.soc.surrey.ac.uk/7/4/2.html.
23. Ortiz-Pelaez A, Pfeiffer DU, Soares-Magalhães RJ and Guitian FJ. Use of social network analysis to characterize the pattern of animal movements in the initial phases of the 2001 foot and mouth disease (FMD) epidemic in the UK. *Prev Vet Med* 2006; 76: 40–55.
24. Newman MEJ. The structure and function of complex networks. *SIAM Rev* 2003; 45: 167–256, http://arxiv.org/abs/condmat/0303516.
25. Barabási AL and Albert R. Emergence of scaling in random networks. *Science* 1999; 286: 509.
26. Watts DJ and Strogatz SH. Collective dynamics of 'small-world' networks. *Nature* 1998; 393: 440–442. doi:10.1038/30918.
27. Erdos P and Renyi A. On the evolution of random graphs. *Publ Math Inst Hungarian Acad Sci* 1960; 5: 17–61.
28. Pastor-Satorras R and Vespignani A. Epidemic spreading in scale-free networks. *Phys Rev Lett* 2001; 86: 3200, doi:10.1103/PhysRevLett.86.3200.
29. Huang CY, Sun CT and Lin HC. Influence of local information on social simulations in small-world network models. *J Artif Soc Soc Simulat* 2005; 8: 8, http://jasss.soc.surrey.ac.uk/8/4/8.html.
30. Barrett CL, Eubank SG and Smith JP. If smallpox strikes Portland. *Sci Am* 2005; 292: 54–61.
31. Barrett CL, Eubank S, Kumar VSA and Marathe MV. Understanding large-scale social and infrastructure networks: a simulation-based approach. *SIAM News* 2004; 37(4): 1–5.
32. Barrett C., Eubank S., and Marathe M. Modeling and Simulation of Large Biological, Information and Socio-Technical Systems: An Interaction Based Approach. *Interactive Computation: The New Paradigm*, 1st edn. 353–392. Berlin: Springer-Verlag, 2006.
33. May RM and Lloyd AL. Infection dynamics on scale-free networks. *Phys Rev E* 2001; 64: 66112.
34. Draief M, Ganesh A and Massoulié L. Thresholds for virus spread on networks. *Ann Appl Probab* 2008; 18: 359–378.
35. Levin SA and Durrett R. From individuals to epidemics. *Phil Trans Biol Sci* 1996; 351: 1615–1621.
36. Davis GF, Yoo M and Baker WE. The small world of the American corporate elite, 1982–2001. *Strat Organ* 2003; 1: 301–326.
37. Sawyer RK. Artificial societies: multiagent systems and the micro-macro link in sociological theory. *Soc Meth Res* 2003; 31: 325–363.
38. Directorate-General of Budget, Accounting, and Statistics. *A preliminary report on year 2000 population and household census in Taiwan*. Taipei, Taiwan 2001.
39. Liu Z, Lai YC and Ye N. Propagation and immunization of infection on general networks with both homogeneous and heterogeneous components. *Phys Rev E* 2003; 67: 31911.
40. Huang CY, Tsai YS, Wen TH. A Network-Based Simulation Architecture for Studying Epidemic Dynamics. *Simulation* 2010; 86: 351–368.

Yu-Shiuan Tsai received his BS and MS in Mathematics from the National Taiwan University, Taiwan, in 2002 and 2005, respectively. He is currently a PhD candidate in the Department of Computer Science, National Chiao Tung University. His current research interests include complex networks and systems, social simulations, and computational epidemiology.

Chung-Yuan Huang received his MS in Computer Information and Science (2000) and his PhD in Computer Science (2005), both from the National Chiao Tung University, Taiwan. He is currently an Associate Professor in the Department of Computer Science and Information Engineering and a member of the Research Center for Emerging Viral Infections at Chang Gung University, Taiwan. His research interests include complex adaptive networks and systems, agent-based modeling and simulation for social science research, and computational epidemiology.

Tzai-Hung Wen received his PhD in Engineering (2006) from the National Taiwan University and is currently an Assistant Professor in the Department of Geography, College of Science, National Taiwan University, Taiwan. He is also a joint faculty member of the Infectious Diseases Research and Education Center at National Taiwan University and Department of Health, Executive Yuan, ROC (Taiwan). His research interests

cover applications of GISs and spatiotemporal modeling in infectious disease epidemiology and evaluation of control strategies for epidemics.

Chuen-Tsai Sun is currently a joint Professor in the Department of Computer Science and Graduate Institute of Education, National Chiao Tung University, Taiwan.

Muh-Yong Yen accomplished his training in infectious diseases at the General Veterans Hospital in 1987. He received further education at Columbia University, USA, in molecular biology, and at the National Sun Yat-Sen University, where he obtained an EMBA. From 2006 to 2009, he was the elected president of the Infection Control Society of Taiwan. He is now Deputy Superintendent of Taipei City Hospital, and Director of the Division for Disease Control and Prevention, Taipei City Government. His field of interests include emerging infectious diseases, infection control, and crisis management.